Mass spectrometry and decay spectroscopy of isomers across the $Z = 82$ shell closure

J. Stanja,[1,*] Ch. Borgmann,[2,†] J. Agramunt,[3] A. Algora,[3,4] D. Beck,[5] K. Blaum,[2] Ch. Böhm,[2] M. Breitenfeldt,[6] T. E. Cocolios,[7,8] L. M. Fraile,[9] F. Herfurth,[5] A. Herlert,[10] M. Kowalska,[7] S. Kreim,[2] D. Lunney,[11] V. Manea,[11] E. Minaya Ramirez,[5,12] S. Naimi,[11,13] D. Neidherr,[5] M. Rosenbusch,[14] L. Schweikhard,[14] G. Simpson,[15] F. Wienholtz,[14] R. N. Wolf,[14] and K. Zuber[1]

[1]*Technische Universität Dresden, 01069 Dresden, Germany*
[2]*Max-Planck-Institut für Kernphysik, 69117 Heidelberg, Germany*
[3]*IFIC, CSIC-Universidad de Valencia, 46071 Valencia, Spain*
[4]*Institute of Nuclear Research of the Hungarian Academy of Sciences, H-4001 Debrecen, Hungary*
[5]*GSI Helmholtzzentrum für Schwerionenforschung GmbH, 64291 Darmstadt, Germany*
[6]*Instituut voor Kern- en Stralingsfysica, 3001 Heverlee, Belgium*
[7]*CERN, 1211 Geneva, Switzerland*
[8]*University of Manchester, Manchester M13 9PL, United Kingdom*
[9]*Grupo de Física Nuclear, Universidad Complutense, 28040 Madrid, Spain*
[10]*FAIR GmbH, 64291 Darmstadt, Germany*
[11]*CSNSM-IN2P3-CNRS, Université Paris-Sud, 91406 Orsay, France*
[12]*Helmholtz-Institut Mainz, 55099 Mainz, Germany*
[13]*SLOWRI Team, Nishina Accelerator-Based Research Center, RIKEN, 2-1 Hirosawa, Wako, Saitama 351-0198, Japan*
[14]*Ernst-Moritz-Arndt-Universität, Institut für Physik, 17487 Greifswald, Germany*
[15]*LPSC, Université Joseph Fourier Grenoble 1, Institut National Polytechnique de Grenoble, CNRS/IN2P3, 38026 Grenoble Cedex, France*

(Received 29 August 2013; published 6 November 2013)

Recent results from a measurement campaign studying the isomerism in neutron-deficient Tl isotopes are presented. The measurements make use of a nuclear spectroscopy setup coupled to the high-resolution Penning-trap mass spectrometer ISOLTRAP at CERN's radioactive ion-beam facility ISOLDE. The mass values of ^{190,194}Tl are improved and a mass-spin-state assignment is carried out. An additional mass measurement of the grandparent nuclide ^{198}At allows the deduction of the spin-state ordering in ^{190}Tl. As a result, the excitation energies of the isomers in both Tl isotopes are determined for the first time to $E_{ex}(^{194}\text{Tl}) = 260(15)$ keV and $E_{ex}(^{190}\text{Tl}) = 89(12)$ keV. Furthermore, this allows anchoring of the ground-state and isomer masses of ^{194}Bi, ^{202}Fr, and ^{206}Ac, which are linked by two independent α-decay chains.

DOI: 10.1103/PhysRevC.88.054304 PACS number(s): 21.10.Dr, 27.80.+w, 37.10.Ty, 82.80.Qx

I. INTRODUCTION

The proximity to the $Z = 82$ shell closure and the existence of isomeric states at only a few hundred kilo–electron volts make neutron-deficient thallium (Tl; $Z = 81$) isotopes interesting cases to test the nuclear shell model. Observations from nuclear charge radii suggest that the Tl isotopes remain spherical for at least $N \geqslant 115$ [1,2]. From the available shell-model orbitals and the ground-state spin of odd-A Pb isotopes, a dominant $\pi s_{1/2} \otimes \nu p_{3/2}$ ground-state configuration for even-A Tl isotopes with $A \leqslant 198$ is expected. However, measurements of magnetic moments point, rather, to a mixed ground-state configuration [3]. The investigation of neutron-deficient Tl isotopes for nuclear structure studies becomes even more interesting with respect to the deformation and shape coexistence which exist in this region [4,5]. These phenomena manifest themselves in the evolution of nuclear observables of the ground state and low-energy levels.

Especially in many of the odd-odd neutron-deficient Tl isotopes the spin-state ordering is not known, and the excitation energies of the isomers are only predicted from systematics.

To address this information a measurement campaign of the isomers in neutron-deficient Tl isotopes was performed at the radioactive ion-beam facility ISOLDE using the Penning-trap mass spectrometer ISOLTRAP [6,7] in combination with its decay-spectroscopy setup [8]. The masses of the individual states can hence be measured and their decay can be studied separately. The technique, which has been used at the JYFLTRAP experiment [9], allows for a unique identification of the spin-state ordering. The success of the measurement is, however, limited by the relative production of each species. While the studies of ^{194}Tl benefited from an indirect production reaction, α-decay chains were exploited for ^{190}Tl. After introduction of the experimental setup in Sec. II, the results of the measurements of ^{190,194}Tl and ^{198}At are presented in Sec. III, and their impact is discussed in Sec. IV.

II. EXPERIMENTAL SETUP

The ion beams in the four individual beam times, two for ^{190}Tl and one each for ^{194}Tl and ^{198}At, were produced at ISOLDE [10] with the settings and production rates listed

*j.stanja@physik.tu-dresden.de
†Present address: Department of Physics and Astronomy, Uppsala University, Box 516, SE-751 05 Uppsala, Sweden.

TABLE I. ISOLDE operational parameters for the individual runs. Listed are the ion source, the ion energy, the magnetic separator, and the production rate. Production rates are given in ions/s at the focal plane of the mass separator and determined either from the ISOLDE Target Group yield measurements or from the measured rates in the experimental setup, corrected for ion transport efficiency. For details see text.

Isotope	Ionization	Ion energy (keV)	Magnetic separator	Production rate (ions/s)
^{190}Tl	Hot plasma	30	HRS	$\sim 1 \times 10^6$
^{190}Tl	Surface + RILIS	50	GPS	$\sim 1 \times 10^8$
^{194}Tl	Surface	40	HRS	$\sim 1 \times 10^4$
^{198}At	Surface + RILIS	50	HRS	$\sim 1 \times 10^3$

in Table I. The proton-induced spallation, using a target made from uranium carbide (UC_x), was followed by surface, hot plasma, or laser ionization. The latter used the resonance ionization laser ion source (RILIS) [11], which, in the case of ^{198}At [12], provided a narrow-band mode [13] which was sufficient to resolve the hyperfine structure by in-source laser spectroscopy. After the ionization process, the ions were accelerated and mass selected with a magnetic separator, either the high-resolution separator HRS or the general-purpose separator GPS. Subsequently, the ions were guided to the ISOLTRAP experiment.

The ISOLTRAP mass-measurement setup [6,7] consists of a radio-frequency quadrupole (RFQ) cooler and buncher [14], a multireflection (MR) time-of-flight (TOF) mass separator (MS) [15], a preparation, and a precision Penning trap, as shown in Fig. 1. The quasicontinuous ion beam from ISOLDE is buffer-gas-cooled and bunched in the RFQ ion trap before being sent as low-energy and low-emittance ion bunches to the subsequent ion traps. The isobaric contaminations in the ion bunches can be removed either in the MR-TOF MS or in the cylindrical preparation Penning trap.

For Tl measurements the mass-selective buffer-gas cooling method in the latter was applied [16]. In the case of astatine, the ISOLDE beam was contaminated mainly with two orders

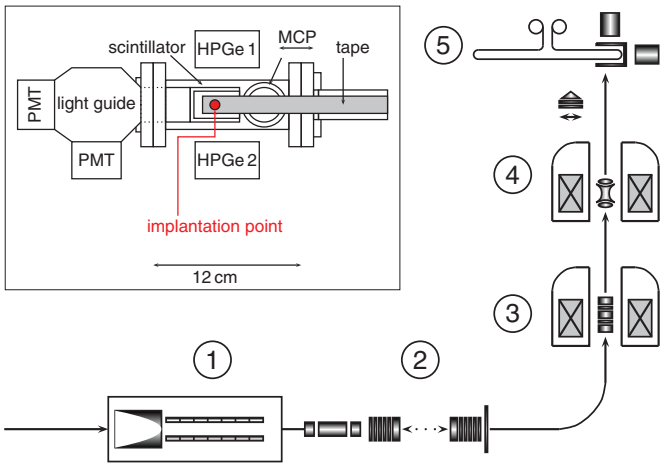

FIG. 1. (Color online) Scheme of the ISOLTRAP setup [6,7], with (1) the RFQ cooler and buncher, (2) the MR-TOF MS with Bradbury-Nielsen gate, (3) the preparation Penning trap, (4) the precision Penning trap, and (5) the decay-station extension. Inset: Schematic top view of the decay station.

of magnitude more ^{198}Tl ions. Thus, the ions were first trapped in the MR-TOF MS to separate the contaminating ions from the ions of interest. The resulting TOF separation of 2 μs allowed to remove the contaminating ions subsequently with a Bradbury-Nielsen gate [17]. Remaining contaminants were removed with the mass-selective buffer-gas cooling method in the preparation Penning trap.

In the hyperbolic precision Penning trap even isomers of a few hundred kilo-electron-volt ($A \gtrsim 150$) excitation energy can be resolved and removed [18–21] and the mass is determined with the TOF ion cyclotron resonance (TOF-ICR) method. To this end, an RF-excitation scheme is applied to the stored ions followed by a TOF measurement [22,23] to determine the cyclotron frequency ν_c of the ion with charge q in magnetic field B, which is linked to its mass m_i according to

$$\nu_c = \frac{1}{2\pi}\frac{qB}{m_i}. \tag{1}$$

The resonance pattern resulting from several tens of measurements is shown in Fig. 2. If the excitation frequency is equal to ν_c the TOF reaches a minimum. With the measurement cycle described above typically an ion transport efficiency of the order of 0.1% is reached, limited mostly by the injection into the RFQ cooler and buncher.

To calibrate the magnetic field during the measurements, an additional measurement of a reference ion with a well-known mass is carried out. The atomic mass m_a of interest is then given by

$$m_a = r(m_{\mathrm{ref},a} - m_e) + m_e, \tag{2}$$

with $r = \nu_{c,\mathrm{ref}}/\nu_c$ the cyclotron frequency ratio, m_e the electron mass, and $m_{\mathrm{ref},a}$ the atomic mass of the reference.

Alternatively, the ISOLTRAP experiment can be used as a purification setup which provides isomerically pure ion samples, which are of great interest for nuclear-decay spectroscopy. Therefore, the ISOLTRAP mass-measurement section was extended by a decay-spectroscopy setup, as shown in Fig. 1, described in detail in [8].

For decay measurements, ion bunches, with up to 30 ions of interest, are transferred to the trap for purification. After ejection from the precision trap the ions, with an energy of a few electron volts, are reaccelerated by a pulsed cavity to 15 keV. Subsequently, they are implanted into an aluminized Mylar tape which is housed in a decay chamber. Any daughter activity can be removed from the decay chamber before implanting a new sample using a tape transport system. At the implantation point the tape is surrounded by a thin

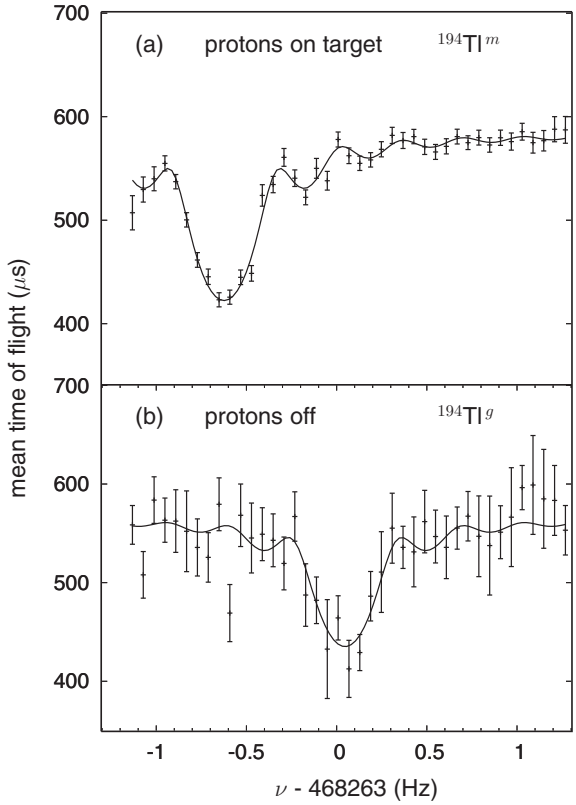

FIG. 2. Resonances obtained for ^{194}Tl with the TOF-ICR method and an excitation time of 3 s in the precision trap. The solid lines are fits of the theoretical line shape to the data. The resonance corresponds to (a) the isomer (protons on) and (b) the ground state (protons off). For details see text.

plastic-scintillator tube which is sensitive to β particles and covers almost 4π of the solid angle. The scintillator is connected to a light guide that distributes the scintillation light to two photomultiplier tubes perpendicular to each other and shielded by mu-metal from the residual magnetic field of the precision-trap magnet. Furthermore, the decay chamber has aluminum walls which are only 1 mm thick and thus allow γ-ray detection with high-purity germanium (HPGe) detectors outside the vacuum but in close geometry (in both cases only a few centimeters from the sample). For the measurements presented here, one HPGe detector with 55% relative efficiency was used for ^{194}Tl and two with 70% and 32% relative efficiency (with respect to a 3 × 3-in. NaI crystal at 1332 keV) were placed in 180° geometry for ^{190}Tl (see inset in Fig. 1). The signals of the photomultiplier tubes and HPGe detectors were recorded with a triggerless digital data acquisition system based on XIA DGF-4C modules [24]. This allowed the construction of coincidences off-line.

III. MEASUREMENTS

Here, the results from a combination of mass and decay measurements for ^{190,194}Tl as well as those from a mass measurement of ^{198}At are presented. The properties of the investigated states of these three nuclides are summarized in Table II.

A. ^{194}Tl

The ground-state spin of ^{194}Tl has previously been assigned 2^- [3]. A (7^+) spin has been tentatively assigned to the isomeric state [29], but its excitation energy has never been reported. During the ^{194}Tl studies with ISOLTRAP, upon proton impact, only one state was produced directly [see Fig. 2(a)]. Additional spin states are fed by decays of heavier species which are produced in the target. If the half-lives are suitable, their yields can be enhanced with respect to the direct production by stopping the proton irradiation on the target regularly. The study of such a case is shown in Fig. 2(b), where the initial state was suppressed and instead a state of lower mass became visible, most likely owing to the decay sequence [26],

$$^{198}\mathrm{Po}^{g} \xrightarrow[t_{1/2}=1.76\ \mathrm{m}]{\alpha} {}^{194}\mathrm{Pb}^{g} \xrightarrow[t_{1/2}=12\ \mathrm{m}]{\mathrm{EC}+\beta^+} {}^{194}\mathrm{Tl}^{g}. \qquad (3)$$

From the electron capture (EC)/β^+ decay of ^{194}Pb, only low-spin states in ^{194}Tl are populated, which subsequently decay to the ^{194}Tl 2^- ground state. Thus, the (7^+) isomeric state is not produced in this case. The production rate for the directly populated state is listed in Table I, while the other state was produced with about an order of magnitude lower yield; hence the larger error bars.

Frequency ratios have been determined for ^{194}Tl$^{g,m+}$ with respect to ^{133}Cs$^+$. The details of the ^{194}Tl^{g} mass determination are given in [30] and [31]. For ^{194}Tl^{m}, six resonances were recorded with the TOF-ICR method, yielding a weighted average frequency ratio of 1.459 470 699 2(310). Here, the statistical uncertainty accounts for 87% of the error, while the remaining systematical uncertainty is caused by a

TABLE II. Mass excess (ME) and Q_{EC} values of ^{190,194}Tl and ^{198}At from the literature [25–27] and values determined in this work by direct mass measurement. The latter are partially included in a recent atomic mass evaluation [28]. Values are given in keV. Extrapolations based on systematics are indicated by superscript asterisks.

Nuclide	Spin	ME		Q_{EC}	
		Literature	This work	Literature	This work
^{190}Tl^{m}	$7^{(+)}$	−24 200*(70*)	−24 289.3(6.4)	7 090(140)	7 081(17)
^{194}Tl^{g}	2^-	−26 830 (140)	−26 937(14)	5 370(140)	5 247(14)
^{194}Tl^{m}	(7^+)	−26 530*(240*)	−26 677.2(3.8)	5 370(140)	5 507(5)
^{198}At^{g}	(3^+)	−6 670(50)	−6 715(6)	8 803(53)	8 758(18)

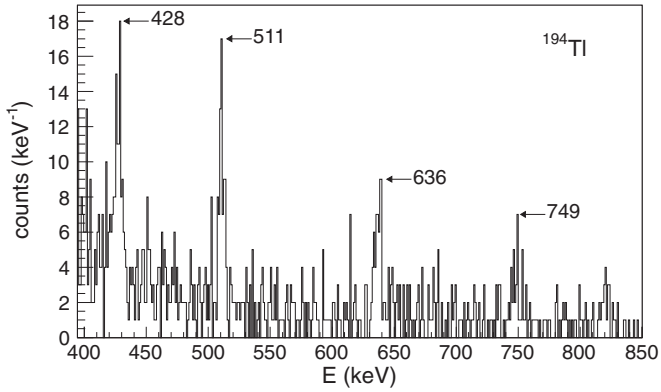

FIG. 3. A β-triggered γ-ray energy spectrum for ^{194}Tl between an HPGe detector and the scintillator at the implantation point after 1.5 h of implantation. The peak at 820 keV does not fit any known transition from the decay of ^{194}Tl.

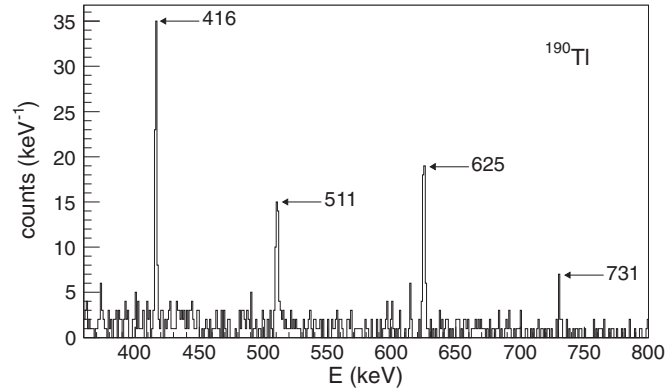

FIG. 4. A β-triggered γ-ray energy spectrum for ^{190}Tl for one HPGe detector at the implantation point after 2×15 min of implantation.

time-dependent shift of the magnetic field, a mass-dependent effect, and a residual systematic uncertainty [32]. The mass of the reference ion ^{133}Cs was taken from [28]. For the isomeric state this results in a mass excess of $-26\,677.2(3.8)$ keV. Upon subtracting the ground-state mass excess from Refs. [30] and [31] the resulting mass difference is 260(15) keV.

To confirm the spin-state ordering, the isomeric state, whose production was an order of magnitude stronger, was investigated with the decay station. In total, two data sets were taken, with 1.5 and 2.5 h of continuous implantation. Owing to the long half-life, $t_{1/2} = 444(77)$ yr [26], of the daughter nucleus ^{194}Hg, no tape movement was required within each data set.

The strongest γ transitions known for the ^{194}Tl decay are at 428.20(25), 636.30(25), and 749.0(3) keV [33]. While the first two transitions are common for both decaying states the latter can be observed only following the decay of the high-spin state. This transition was clearly visible in the spectra (see Fig. 3), meaning that the isomer is indeed the high-spin state.

To estimate the purity of the ion sample the measured intensity ratios for the three above transitions were compared to literature values (see Table III). This comparison limits the admixture of the low-spin state to max. 10%. Thus, frequency shifts in the mass measurement owing to this admixture can be neglected [18]. The half-life of 37(6) min determined from the three γ lines is in agreement with the literature half-life of both states and thus cannot provide additional information.

To summarize, the results from mass and decay measurements for ^{194}Tl confirmed the ordering of the two β-decaying states. For the first time, the excitation energy of the (7^+) isomer was determined to be 260(15) keV. In addition, the uncertainties in the Q_{EC} values for the decays of both states to the ground state of ^{194}Hg, with the mass excess taken from [28], were reduced by an order of magnitude (see Table II).

TABLE III. Comparison of literature [26,27] and measured intensity ratios for the most intense γ-ray transitions from the decay of low- and high-spin states in ^{194}Tl and ^{190}Tl, respectively.

State	^{194}Tl		^{190}Tl	
	$I(428)/I(636)$	$I(428)/I(749)$	$I(416)/I(625)$	$I(416)/I(731)$
Low spin	8.2(1.3)	—	7.1(1.9)	—
High spin	1.0(1)	1.3(1)	1.1(1)	2.4(3)
This work	1.0(2)	1.2(3)	1.1(2)	2.0(4)

B. ^{190}Tl

In ^{190}Tl, a $2^{(-)}$ and a $7^{(+)}$ state were assigned [2] but their order is unknown [27]. During the present measurement, only one state was produced upon proton impact, with the production rate given in Table I. For this state a mass excess of $-24\,289.3(6.4)$ keV was determined. For details, see [30] and [31]. The identification of the spin state was carried out with the ISOLTRAP decay station. In total, nine data sets have been recorded, each with a continuous implantation of about 15 min. Different γ-ray transitions known from ^{190}Tl, the most intense at 416.4(2), 625.4(2), and 731.1(2) keV [36], have been identified in the spectra (see Fig. 4). Again, the first two transitions are common for both states and the latter can only be observed from the decay of the high-spin state. A comparison of the measured γ-ray intensity ratios with the literature values as for ^{194}Tl proves the presence of only the $7^{(+)}$ state (see Table III). This is supported by the half-life, which was determined from the three γ-ray transitions to be 3.6(3) min, in agreement with the previously reported value for the high-spin state. Thus, the combination of mass and decay measurements yields a precise mass value for the high-spin state.

To finally answer the question of state ordering, additional information is required. As shown in Fig. 5, the $2^{(-)}$ and $7^{(+)}$ states of ^{190}Tl belong to two independent α-decay chains. By measuring the mass of the (3^+) state of any of the linked nuclides, the state ordering in ^{190}Tl can be extracted. Data from another ISOLTRAP measurement were used, where ^{198}At was produced and laser-ionized. To ionize a selected species, laser beams tuned to specific atomic transitions excite an electron stepwise until it is ejected. The atomic hyperfine structure can be measured by scanning the frequency of one of these laser transitions and measuring the intensity, as shown in Fig. 6. This method allowed an unambiguous state assignment as demonstrated first in combination with mass spectrometry for ^{68,70}Cu [20,41]. Because the laser frequency was recorded

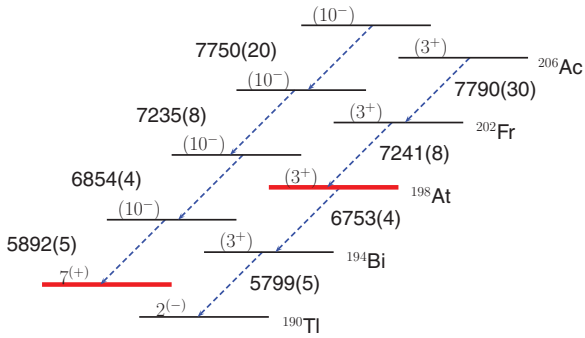

FIG. 5. (Color online) Independent α-decay chains for the two states in ^{190}Tl. The state ordering in ^{190}Tl and all mother nuclei as well as their masses can be extracted from the direct mass measurements of ISOLTRAP [thick horizontal (red) lines] and the known α energies [dashed ((blue) lines [26,27,34,35]. Energies are given in keV.

in units of inverse centimeters, the corresponding quantity wave number (cm^{-1}) is used. For the (3^+) state in ^{198}At three TOF-ICR resonances with the laser tuned to the wave number 15 411.1 cm^{-1} were recorded, again with ^{133}Cs as reference ion. As can be deduced from Fig. 6, this wave number corresponds to a dominant (3^+) state of ^{198}At. In addition, the wave number was tuned to 15 411.2 cm^{-1} resulting in a mixture of the (3^+) and (10^-) of ^{198}At (see Fig. 6). At this wave number a double resonance was recorded, which was considered in the mass evaluation of the (3^+) state. The resulting weighted average frequency ratio for the ground state is $r = 1.489\,728\,656\,1(470)$, which yields a mass excess of $-6715(6)$ keV. For the isomeric state, a frequency ratio of $r = 1.489\,731\,099\,3(2900)$, again with respect to ^{133}Cs, has been determined from the double resonance. This equals a mass excess of $-6412(36)$ keV.

Based on the ISOLTRAP mass values for the $7^{(+)}$ state in ^{190}Tl and for the (3^+) state in ^{198}At, respectively, the masses of all other members in the α-decay chains are fully determined, as listed in Table IV. The mass-excess values of the excited states are included in the recent atomic mass evaluation [28], which is not the case for the ground states. For ^{190}Tl the $2^{(-)}$

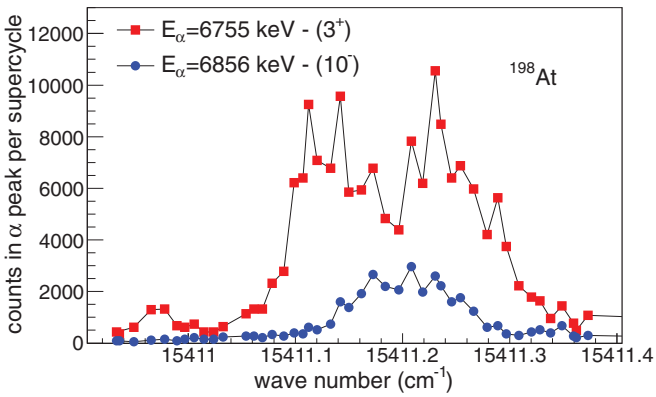

FIG. 6. (Color online) Hyperfine-structure scan for ^{198}At resulting from a dedicated experiment [37] with the use of the Windmill α-decay setup [38]. For individual states the counts at a fixed α energy were measured while varying the wave number.

TABLE IV. Mass excess of the members of two α-decay chains between ^{190}Tl and ^{206}Ac from the literature [25] and determined in this work using only the mass values of the $7^{(+)}$ state in ^{190}Tl, the (3^+) state in ^{198}At, and the known α-decay energies from the literature [26,27,34,35]. Excitation energies of the isomers to their respective ground state are also given. Energies are given in keV; values extrapolated from systematics are indicated by superscript asterisks.

Nuclide	Spin	ME		E_{ex}:
		Literature	This work	This work
^{190}Tl^g	$2^{(-)}$	$-24\,330(50)$[a]	$-24\,378(10)$	—
^{190}Tl^m	$7^{(+)}$	$-24\,200^*(70^*)$	$-24\,289.3(6.4)$	89(12)
^{194}Bi^g	(3^+)	$-15\,990(50)$	$-16\,032(8)$	—
^{194}Bi^m	(10^-)	$-15\,760^*(70^*)$	$-15\,848(9)$	184(12)
^{198}At^g	(3^+)	$-6\,670(50)$	$-6\,715(6)$	—
^{198}At^m	(10^-)	$-6\,340^*(70^*)$	$-6\,428(10)$	287(12)
^{202}Fr^g	(3^+)	3 140(50)	3 097(11)	—
^{202}Fr^m	(10^-)	3 470*(70*)	3 378(13)	281(17)
^{206}Ac^g	(3^+)	13 510(70)	13467(32)	—
^{206}Ac^m	(10^-)	13 800*(80*)	13 707(24)	240(40)

[a]It is noted that the literature value agrees with the mass excess of the values of both the ground and the isomeric state in ^{190}Tl within the uncertainty [39,40].

state is identified as the ground state and the excitation energy of the $7^{(+)}$ isomer is 89(12) keV. Also, in the other nuclides linked by the α-decay chains the state ordering is clarified, with the respective low-spin state as the ground state and the high-spin state as the isomeric state. The excitation energies are listed in Table IV. Thereby, the result for ^{198}At^m is in agreement with that from the double resonance.

IV. DISCUSSION

The Tl isotopes are only one proton away from the $Z = 82$ shell closure. Thus, the spherical single-particle shell model should suitably describe the evolution of their properties, for example, spin and parity [29]. From the available shell-model orbitals and the systematics of the neighboring Pb isotopic chain, the unpaired proton and neutron in the even-A Tl isotopes are expected to occupy, in their ground state, the $\pi s_{1/2}$ and $\nu p_{3/2}$ orbitals for $A \leqslant 198$. The coupling of these unpaired nucleons yields a doublet of states with spin 1^-, 2^-. The observation of a 2^- ground state in odd-odd neutron-deficient Tl isotopes supports this description [3]. It was, however noted, that an admixture of a $\pi s_{1/2} \otimes \nu f_{5/2}$ configuration becomes likely for more neutron-deficient Tl isotopes [3], as the magnetic moments lie in between the two empirical moments calculated from the additivity relation from [46] (see Fig. 7). Although, for $N \leqslant 117$, the magnetic moments of the 2^- state start to approach the empirical value for a $\pi s_{1/2} \otimes \nu p_{3/2}$ configuration, they do not reach it, at least down to $N = 103$. The 7^+ states in the neutron-deficient Tl isotopes arise from a hole excitation to the neutron $i_{13/2}$ orbital and coupling to the $s_{1/2}$ proton, leading to a doublet of states with spins 6^+ and 7^+. Contrary to the 2^- states, the magnetic moments of the 7^+ states suggest that they can be described

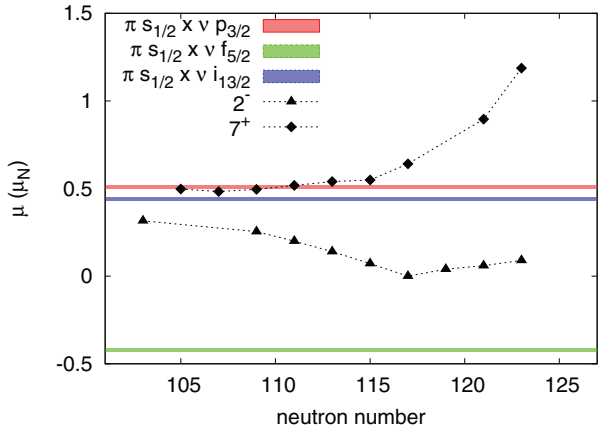

FIG. 7. (Color online) Magnetic moments for even-A neutron-deficient Tl isotopes [1–3,42–45]. Shaded horizontal bands indicate empirical moments calculated using the additivity relation from [46].

by a pure configuration for $N \leqslant 115$ as would be expected, owing to the unique-parity nature of the $i_{13/2}$ orbit.

The excitation-energy systematics for the Tl isomers including the new values for ^{194}Tl and ^{190}Tl are shown in Fig. 8. For $N \geqslant 117$ a behavior similar to the $13/2^+ \rightarrow 5/2^-$ spacing in odd-A Pb isotopes was found [47]. It was noted in [29] that the energy gap widens at $N = 115$. This deviation continues for smaller N, as shown by this work. Taking also the $13/2^+ \rightarrow 3/2^-$ level spacings for Pb isotopes into account, it seems that the Tl isotopes represent an intermediate situation between the two configurations, which might be attributed to the mixed nature of the ground-state.

In addition, the systematics show that the level spacing between the 2^- and the 7^+ state decreases with smaller N,

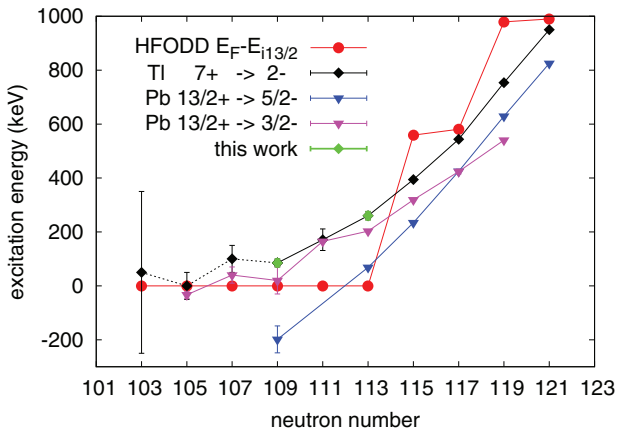

FIG. 8. (Color online) Systematics of the excitation energy of the isomeric states in even-A neutron-deficient Tl isotopes (black diamonds) compared to energy-level spacings in neutron-deficient Pb isotopes (magenta and blue triangles). Data are taken from [28], [48], [49], and this work (green diamonds). Note that the excitation energies of the isomers in Tl isotopes with $N < 109$ (dotted line) are extrapolated values. The (red) circles represent the energy difference between the Fermi level and the neutron $i_{13/2}$ level as obtained from a spherical HFB calculation with the SKM* interaction using the HFODD code [50,51].

which points to a level inversion halfway between the shell closure at $N = 82$ and that at $N = 126$, as discussed for Tl in [52]. In the neighboring Hg this inversion is indeed observed [4]. The decrease in excitation energy can be qualitatively understood from the single-particle picture, in which the neutron orbitals $s_{1/2}$, $f_{5/2}$, and $p_{3/2}$ are successively emptied with decreasing neutron number. Thus, the Fermi level gets closer to the $i_{13/2}$ orbital and the energy required to create a $i_{13/2}$ hole is reduced.

The difference between the Fermi level and the $i_{13/2}$ orbital, resulting from a calculation using a spherical Hartree-Fock-Bogoliubov (HFB) model with the SKM* interaction in the HFODD code [50,51], is also shown in Fig. 8. However, within this model the valence neutron is expected to occupy the $i_{13/2}$ level in the ground state for $N \leqslant 113$, which is not observed at least for $N \geqslant 109$, as shown in this work. Here it becomes noticeable that the spherical shell model yields, in fact, an oversimplified description of the Tl isotopes. The observed state ordering can, however, be understood in terms of either nucleon scattering driven by shape coexistence [4] or the Nilsson model assuming a slight oblate deformation. In the latter case the degeneracy of the neutron $i_{13/2}$ orbital is lifted and its members 3/2[651] and 5/2[642] can account for the ground state, while the 13/2[606] member, which is lowered the most in energy, forms the isomer.

Looking at other nuclides affected by this work, ^{202}Fr is of particular interest. The binding energy is an important input parameter for investigating transitional regions, which has been shown for the isotopic chain of platinum [53]. Around $N = 112$, ^{202}Fr was the last nucleus in the chain of francium isotopes with an unknown mass. Properties of heavy nuclei, such as signatures for transitional nuclei or development of collectivity are treated in [54]. The low-uncertainty result and the unambiguous ordering of states in ^{202}Fr allow for a study of these phenomena. Furthermore, its ground and isomeric state have recently been studied in the framework of shape coexistence by collinear laser spectroscopy [55] and with respect to EC delayed fission [56], while it is not known whether the ground or isomeric state undergoes this decay. The fission probability depends on, besides the fission barrier of the daughter nucleus, the Q value of the mother nucleus [57]. More precise mass and excitation-energy values for ^{202}Fr are thus of particular interest for fission studies and might help clarify the situation.

V. SUMMARY

Measurements of even-A neutron-deficient Tl isotopes ^{190,194}Tl have been presented, which combine high-precision mass measurements with nuclear-decay spectroscopy. This combination allows the assignment of known long-lived states to masses. The masses of ^{190}Tl^m, ^{194}Tl^g, ^{194}Tl^m, and ^{198}At^g have been measured directly and their uncertainties were decreased significantly. For the first time, the excitation energy of the isomer in ^{194}Tl has been determined. By the additional mass measurement of the (3^+) state in ^{198}At and the subsequent exploitation of the α-decay link across the $Z = 82$ shell closure, the ground- and isomeric-state ordering in ^{190}Tl has been clarified and the excitation energy of the isomer

deduced. The ground-state and isomer masses, as well as the spin-state ordering, of all other nuclides linked by these decay chains have also been determined. For the Tl isotopes, the resulting spin-state ordering can be understood by a deformed description despite the proximity to the $Z = 82$ shell closure, which is also supported by the level-spacing systematics. In addition, the latter points to a possible level inversion around $N = 105$.

ACKNOWLEDGMENTS

We thank the ISOLDE Collaboration for providing the beams and the RILIS and Windmill teams for producing and identifying the isomeric beam of ^{198}At. We thank Piet van Duppen and Mark Huyse for discussions on α-decay chains. We thank Phil Walker for comments on the manuscript. Furthermore, we thank Lauriane Fouché for her assistance during her internship. This work comprises part of the Ph.D. theses of J. Stanja and Ch. Borgmann. This work was supported by the German Federal Ministry for Education and Research (BMBF) (Grant Nos. 05P09ODCIA, 05P09HGFNE, 05P12HGCI1, 05P12HGFNE, and 06MZ215), a Marie Curie Actions grant (No. MEIF-CT-2006-042114, EU FP6 program), the Max-Planck Society, the Helmholtz Alliance, the European Union seventh framework through ENSAR (Contract No. 262010), the French IN2P3, the Spanish MICINN (Grant Nos. FPA-2010-17142 and FPA-2011-24553), the UK Science and Technology Facilities Council (STFC), and the Robert-Bosch-Foundation.

[1] J. A. Bounds *et al.*, Phys. Rev. C **36**, 2560 (1987).
[2] R. Menges *et al.*, Z. Phys. A **341**, 475 (1992).
[3] C. Ekström, G. Wannberg, and Y. S. Shishodia, Hyp. Interact. **1**, 437 (1975).
[4] K. Heyde and J. L. Wood, Rev. Mod. Phys. **83**, 1467 (2011).
[5] A. N. Andreyev *et al.*, Nature **405**, 430 (2000).
[6] M. Mukherjee *et al.*, Eur. Phys. J. A **35**, 31 (2008).
[7] S. Kreim *et al.*, Nucl. Instr. Methods Phys. Res. Sec. B Proc., (2013), doi: 10.1016/j.nimb.2013.07.072.
[8] M. Kowalska *et al.*, Nucl. Inst. Methods A **689**, 102 (2012).
[9] A. Kankainen *et al.*, Phys. Rev. C **87**, 024307 (2013).
[10] E. Kugler, Hyp. Interact. **129**, 23 (2000).
[11] V. N. Fedosseev *et al.*, Rev. Sci. Instr. **83**, 02A903 (2012).
[12] S. Rothe *et al.*, Nature Commun. **4**, 1835 (2013).
[13] B. Marsh *et al.*, Nucl. Instr. Methods Phys. Res. Sec. B Proc., (2013), doi: 10.1016/j.nimb.2013.07.070.
[14] F. Herfurth *et al.*, Nucl. Instr. Methods Phys. Res. Sec. A **469**, 254 (2001).
[15] R. N. Wolf *et al.*, Int. J. Mass. Spectrom. **349**, 123 (2013).
[16] G. Savard *et al.*, Phys. Lett. A **158**, 247 (1991).
[17] N. Bradbury and R. Nielsen, Phys. Rev. **49**, 388 (1936).
[18] G. Bollen *et al.*, Phys. Rev. C **46**, R2140 (1992).
[19] S. Schwarz *et al.*, Nucl. Phys. A **693**, 533 (2001).
[20] J. Van Roosbroek *et al.*, Phys. Rev. Lett. **92**, 112501 (2004).
[21] Ch. Weber *et al.*, Nucl. Phys. A **803**, 1 (2008).
[22] G. Gräff, H. Kalinowsky, and J. Traut, Z. Phys. A **297**, 35 (1980).
[23] M. König *et al.*, Int. J. Mass Spectrom. Ion. Process. **142**, 95 (1995).
[24] XIA, www.xia.com, October (2013).
[25] G. Audi, A. H. Wapstra, and C. Thibault, Nucl. Phys. A **729**, 337 (2003).
[26] B. Singh, Nucl. Data Sheets **107**, 1531 (2006).
[27] B. Singh, Nucl. Data Sheets **99**, 275 (2003).
[28] G. Audi *et al.*, Chin. Phys. C **36**, 1287 (2012).
[29] B. Jung and G. Andersson, Nucl. Phys. **15**, 108 (1960).
[30] Ch. Borgmann, Ph.D. thesis, University of Heidelberg (2012), http://www.ub.uni-heidelberg.de/archiv/13925.
[31] Ch. Böhm *et al.* (unpublished).
[32] A. Kellerbauer *et al.*, Eur. Phys. J. D **22**, 53 (2003).
[33] B. Amov *et al.*, Sov. J. Nucl. Phys. **16**, 487 (1973).
[34] H. Xialong, Nucl. Data Sheets **110**, 2533 (2009).
[35] S. Zhu, Nucl. Data Sheets **109**, 699 (2008).
[36] Y. Vandlik *et al.*, Izv. Akad. Nauk SSSR, Ser. Fiz. **34**, 1656 (1970).
[37] A. N. Andreyev *et al.*, *CERN-INTC-2012-001, INTC-P-319* (2012), http://cds.cern.ch/record/1410652/files; A. N. Andreyev *et al.*, *CERN-INTC-2013-002, INTC-P-319-ADD-1* (2013), http://cds.cern.ch/record/1551259/files.
[38] A. N. Andreyev *et al.*, Phys. Rev. Lett. **105**, 252502 (2010).
[39] T. Radon *et al.*, Nucl. Phys. A **677**, 75 (2000).
[40] Yu. A. Litvinov *et al.*, Nucl. Phys. A **756**, 3 (2005).
[41] K. Blaum *et al.*, Europhys. Lett. **67**, 586 (2004).
[42] R. Neugart *et al.*, Phys. Rev. Lett. **55**, 1559 (1985).
[43] H. A. Schuessler *et al.*, Hyp. Interact. **74**, 13 (1992).
[44] H. A. Schuessler *et al.*, Nucl. Instr. Methods Phys. Res. Sec. A **352**, 583 (1995).
[45] A. E. Barzakh *et al.*, Phys. Rev. C **88**, 024315 (2013).
[46] G. Neyens, Rep. Prog. Phys. **66**, 633 (2003).
[47] I. Bergström and G. Andersson, Ark. Fys. **12**, 415 (1957).
[48] ENSDF, www.nndc.bnl.gov/ensdf/, October (2013).
[49] T. E. Cocolios *et al.*, J. Phys. G **37**, 125103 (2010).
[50] N. Schunk *et al.*, Comp. Phys. Commun. **183**, 166 (2012).
[51] J. Bartel *et al.*, Nucl. Phys. A **386**, 79 (1982).
[52] J. A. Bounds *et al.*, Phys. Rev. Lett. **55**, 2269 (1985).
[53] J. E. Garcia Ramos *et al.*, Nucl. Phys. A **688**, 735 (2001).
[54] R. F. Casten, D. S. Brenner, and P. E. Haustein, Phys. Rev. Lett. **58**, 658 (1987).
[55] T. E. Cocolios *et al.*, Nucl. Instr. Methods Phys. Res. Sec. B (2013), doi: 10.1016/j.nimb.2013.05.088.
[56] A. N. Andreyev *et al.*, *CERN-INTC-2011-006, INTC-P-235-ADD-2* (2011).
[57] H. L. Hall and D. C. Hoffmann, Annu. Rev. Nucl. Part. Sci. **42**, 147 (1992).